Selective laser sintering of cement with polyamide 12

D.T. Pham, S.A. Aldahsh, A.M. Mousah
The Manufacturing Engineering Centre (MEC), Cardiff University, UK

Abstract: Selective laser sintering is used to create new composite material from cement additives and polyamide 12. The effects of cement on the mechanical properties of the sintered specimens are being investigated. The investigation uses tensile, flexural, and compression testing methods to measure alterations in the mechanical properties of sintered specimens. In addition, the influence of energy density (controlled by laser power, laser speed and scan-spacing) on the dimensions, density, mechanical properties and morphology of sintering specimens is examined. The optimum energy density for producing parts with maximum density and strength has been determined experimentally. The results show that the mechanical properties of the sintered specimens can be significantly improved with the addition of cement, while there is a certain degree of improvement in tensile strength.

Keywords: Rapid Prototype (RP), Selective Laser Sintering (SLS), Polyamide 12 (PA12), Portland cement, Scanning Electron Microscopy (SEM)

1 Introduction

Selective Laser Sintering (SLS) is one of the commonest rapid prototype techniques. It was developed and originally patented by the University of Texas at Austin and was licensed to DTM Corporation. DTM introduced the first commercially available system in 1992, and the latest SLS system by DTM is the Sinterstation 2500 Plus (Kai and Fai, 1997; Pham and Dimov, 2000).

SLS employs powder-processing in the construction of parts. In this process, many types of powder can be used including polymers, ceramics, metals and composites. SLS parts are fabricated by the heat of an infrared laser beam so that the surface tension of the particles is overcome and they fuse together. The powder is supplied by two feed cartridges which supply a thin layer of powder over the build area using a rotating roller. The build area is also supported by a moveable piston (Pham and Dimov, 2003).

The SLS process starts by transferring CAD data files in STL file format to the SLS machine where they are sliced. Build parameters and guidance of the laser are controlled by the data which is processed by a computer system. As well as this, the computer system is used to control nitrogen which creates an inert atmosphere to eliminate the possibility of powder oxidation and explosion. This is followed by heating the powder to a temperature just below the melting point of the material using a heater which is located above the part-bed, in order to minimize thermal distortion and heat stress to the lowest possible degree; prevent the fabrication part from warping and facilitate fusion to the previous layer. The temperature of the powder-feed cartridges is controlled to allow powder to be moved freely by a rotating roller. A very thin layer (between 100 μm to 125μm) is spread by the roller across the part build. The speed of the roller transverse is an adjustable machine parameter (Kumar and Dutta, 1997; Yusoff, 2007).

The SLS machine uses a CO2 laser with up to 50 watt power (Kai and Fai, 1997). The laser beam is guided by two mirrors to the surface of the powder build area to scan specific areas of the powder which correspond to a slice through the object's design geometry. The interaction of the laser beam with the powder, fuses particles to produce the first layer of the LS parts (Neal, 1994; Yusoff, 2007). The part-build cylinder lowers slightly and one of the feed cartridge rises for the next layer of powder to be added, and the process continues until the part is completely fabricated. The sinter powder forms the part while the unsintered powder remains in the part-build during fabrication to surround and support it.

One of the main advantages of the SLS process is that numerous materials and indeed, any material that can be triturated, may be used in the SLS process via a low melting temperature point binder such as a polymer for a high melting point phase to produce a geometrically accurate sintered part (Vail et al., 1996; Hon and Gill, 2003) Consequently the possibility of creating types of materials through SLS might not be feasible using other means. The flexibility of material and shape which SLS technology produces might have practical and effective applications in specific areas.(Maeda and Childs, 2004). Thermoplastics such as polyamide 12 (PA12) have been developed as SLS materials for different applications. However, the focus of the research to create new composite material from cement additive with polyamide 12 so as to improve

the mechanical properties of the sintered specimen through the addition of cement, as well as considerably reduce cost because the price of polyamide is very high. Addition of rigid particles to polymers can produce a number of attractive effects in the mechanical properties of specimens such as increased flexural strength, compression, rigidity, improvement in fracture toughness, creep resistance and, in some cases, tensile strength (Gill and Hon, 2004). The material specifications are listed in Table 1.

Table 1 Material specifications

Powder properties	Portland cement	PA 2200
Average grain size (μm)	15	58
Bulk density (g/cm³)	1.142	0.484
Particle shape	Irregular	Irregular
Melting temperature (C)	1400	185

This paper presents a theory of sintering process of PA12-cement composite and between polyamide particles as well. An experimental study of the tensile, flexural, compression and density specimens to determine the effects of varying the energy density generated by the laser and the effect of varying the proportion of composite cement material to polyamide 12 on the density and mechanical properties of sintered specimens. Explain the effects of various energy densities on composite material properties by examining the physical construction of the specimens.

3 Theory

3.1 Sintering process of PA12-cement composite

PA12 is a crystalline polymer with low melted viscosity. In their initial state during the sintering process, the Portland cement particles are homogeneously distributed through the larger polyamide grains. At the first stage of the SLS process (see Figure 1.a) the polymer/ cement powder mixture is exposed to CO2 laser radiation. The PA12 subsequently absorbs the laser energy and melts. The low melted viscosity is positive for PA12 flowing in the sintering layer, so at the second stage of the SLS process the cement particles are surrounded by the PA12 melt. During this local melting process the small cement particles enter the polymer grain (see Figure 1.b), while melting additional regions of the polymer. This is a possible explanation for the observation that cement particles could barely be detected by SEM at the surface and fracture surface of sintered parts. At the third stage, as a result of the complete melting of the polymer, the formation of 'sintering necks' from one polymer particle to another is started (see Figure 1.c) and causes viscous flow to occur (Ajoku et al., 2006). Viscous sintering was first explored by Frenkel (Beamam et al., 1997). Frenkel used a model for viscous sintering to describe the neck growth between two particles.

$$\left(\frac{x}{r}\right)^2 = \frac{3}{2}\left(\frac{\sigma t}{r\eta}\right) \qquad (1)$$

Where x is half the thickness of the neck formed between contiguous particles, r is the radius of the particle, t represents the time needed for sintering, and ηo is the melt viscosity.

At the last stage (see Figure 1.d), the laser power has left one region for another and the polymer starts to cool down, after that crystallisation process starts.

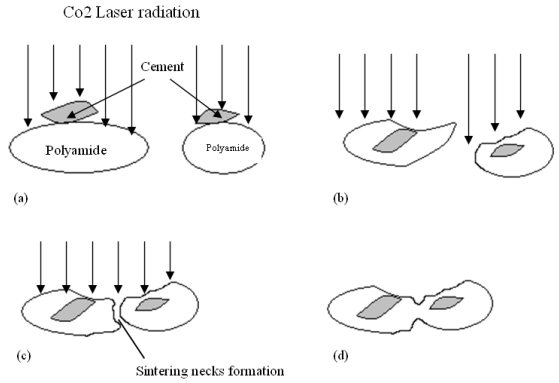

Figure 1 States of the sintering process for SLS. (a) State one: laser energy absorption by PA12 particles; (b) State two: cement particles are surrounded by the PA12 melt; (c) State three: the PA12 particles are completely melted and sintering necks start to form; (d) Final state: laser exposure is carried out and the sintered layer is begun.

3 Experimentation

3.1 Material

The polyamide used was PA12-based powder PA2200 supplied by EOS, which is an ultrafine powder of polyamide 12 with a narrow particle size distribution and nearly round particle shape. The Cement used was Portland cement defined as adhesive material capable of joining fragments or masses of solid substance to a compact whole. The raw materials commonly used to make the Portland cement are limestone or chalk and clay

or shale. Limestone and chalk usually contains significant quantities of component of CaO which is represent the major composition of Portland cement clinker. In regard to clay and shale normally contains major quantities of compounds of SiO2, Al2O3, Fe2O3. Widespread availability of the limestone and shale make Portland cement depressed cost (Lea, 1970; Barnes, 1983; Shirley, 1986). The material specifications for both PA12 and Portland cement are listed in Table 1 while Figure(2) shows scanning electron microscopy (SEM) micrographs of both types of powder is stated as irregular and it is observed that the Portland cement more angular in shape when compared to the PA12.

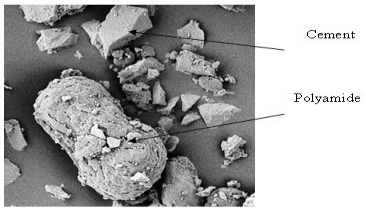

Figure 2 (SEM) Electron micrograph scans of PA12 and cement

3.2 Equipment used

All test specimens were built on a DTM Sinterstation 2000 machine using composite material of PA12-cement. Directions in the build chamber of the SLS machine are *x*-axis is parallel to the front of the machine, while the *y* axis is perpendicular to *x*-axis. The top plane of the powder bed is then the *x*–*y*-plane of the build chamber and the *z*-axis is perpendicular to the *x*–*y*-plane. The mechanical properties tests of the SLS specimens were examined using a Testomeric M500 machine with a range of load 0 to 25 KN, accuracy +/- 0.5% and range of speed 0.001 to 1000 mm/min, all tests were conducted in a room temperature. Cement and PA12 were mechanically mixed in a Drum mixer BS 125 with a capacity 150 L and speed of mixing 30 r.p.m. Composite powder have been sifted by an intensive shaking procedure using VORTI-SIV pilot RBF-15. The particle size and distribution of cement and PA12 powder and sintered substrates were studied using optical microscope with OmniMet software and Scanning Electron Microscope (SEM) at a voltage 2-5 kV using a ZEIZZ 1540 XB. Agar Auto Sputter Coater used for gold coating of the specimens.

3.3 Sample preparation

Composite of cement and PA12 were sifted by an intensive shaking procedure using VORTI-SIV sifter to avoid agglomerates of powder after that composite powder were mechanically mixed in a determinate formulation in a high-speed mixer for 20 min to obtain homogeneous powder mixtures and uniform colour of the mixtures, then transfer the blended powder onto sinterstation 2000 into two feed cartridges. The sintering condition was adjusted by changing the applied laser power between 4.5 and 8 Watt, with laser scanning speed 914 mm/s, scan spacing 0.15 mm, layer thickness 0.1 mm and part bed temperature 177-178° C. After parts sintered the parts were removed from the parts cake and cleaned manually by brush then use sandblasting and pressurised air to remove remnants of the powder on the surface of part. The energy density applied to the SLS parts were calculated using Eq. (2). The sintered parts are then observed using an SEM. As the samples are not conductive material, gold coating is needed to improve the electron conductivity before capturing images into the Cam Scan.

$$ED = \frac{P}{LS * SCSP} \qquad (2)$$

3.4 Measurement and test specimens

The tensile, flexural and compression specimens were tested using a Testomeric M500 machine and were determined with reference to ISO 527.2, ISO 178 and ISO 604 respectively. The tensile specimens were dog-bone shaped and the test speed was 5mm/min. The flexural specimens were 80-10-4 mm, the span was 60 mm and the test speed was 2mm/min. The compression specimens were 10 - 10-4 mm and the test speed was 5mm/min. The density of the material was assessed by building density specimens. The density specimens were 30 - 10-4 mm determined with reference to ISO 1183-3. The dimensions of the specimens were obtained using a micrometer, each dimension was measured three times and then an average dimension was connected with each part. Once the density specimens were measured and weighed, the obvious density was found by dividing mass by volume. The cross-sectional area (CSA) value was developed from the average part thickness and width per ED and so the CSA of the part is important as it is required in calculating the tensile and flexural. The intended CSA for all the parts was 40mm².

4 Results

4.1 Sintering part dimensions and density

Figure 3 shows the part length, width, thickness and the density results obtained, as opposed to their ED. To investigate the effect of the ED on the dimensions and the density of the test specimens, three different measurements of the specimens were taken: length, width and thickness. Figure 3a shows the part length increased by raising energy density. All parts were somewhat smaller than the intended part length of 30 mm except when the highest energy density 0.058 J/mm² was exceeded. As shown in Figure 3b, the required width of 10mm was reached and exceeded by the ED > 0.043 J/mm², and in a similar way, part widths increased with rising energy density. Figure 3c shows the part thickness on the verge of reaching the intended part thickness of 4mm but discontinued at a maximum value with 0.051 J/mm² of ED which consequently initiated a decrease relative to increased energy density. Figure 3d displays variations in density amongst the samples correlating to energy density. When ED is < 0.051 J/mm², the density of the composite increased with increasing ED, and then gradually decreased with increasing ED.

From the results, it can be concluded that ED has an effect on the dimensions and density of the SLS parts of composite material. The parts' dimensions increased relative to increased ED. The parts' thickness yielded values closer to the desired thickness of 4 mm. However, the desired thickness was not reached due to shrinkage of the sintering part during cooling. In addition, the thickness dimensions were controlled by the height of the powder layer. While the parts' length and width were unlike the part thickness, the length and width values reached and exceeded their desired values due to the laser which controlled the length and width dimensions. In general, the increase in part dimensions as a result of ED may be explained by the increase in ED leading to growth in the amount of conduction through the powder, thus causing excess powder particles to melt and fuse, resulting in extra length, width and, to some extent, thickness.

Where the density of the parts is concerned, their dimensions increased due to raised ED, which to some extent causes, density to increase at optimum energy density and then decrease with raised ED. At ED levels in excess of the optimum, the binder in the composite material degrades and evaporates due to excess heat from the laser power.

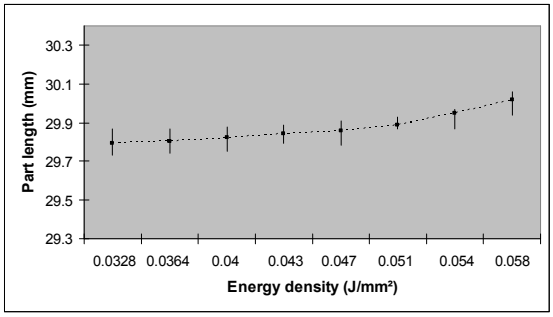

(a)

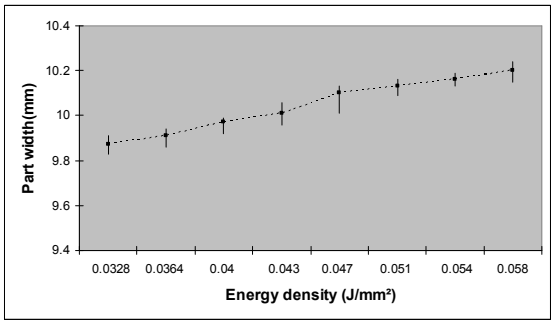

(b)

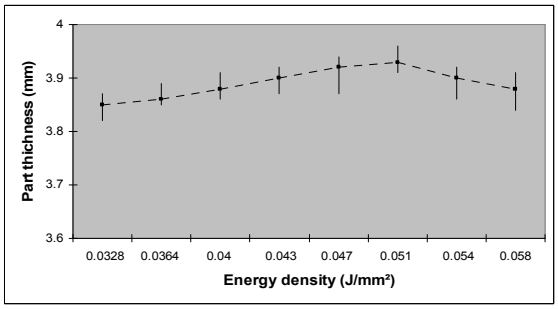

(c)

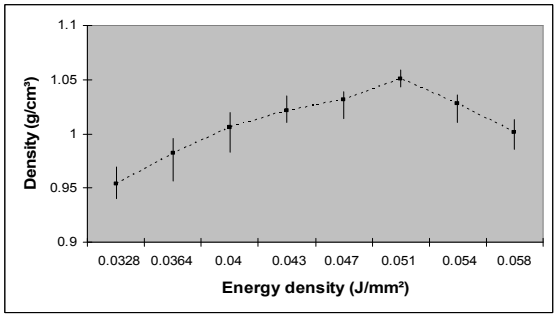

(d)

Figure 3 Variation energy density with (a) length, (b) width, (c) thickness, (d) density

4.2 mechanical properties

The effects of various energy densities and proportions of cement on the mechanical properties of SLS parts are shown in figures 3 to 7 respectively. These show the average, maximum and minimum results in terms of ultimate tensile strength (UTS), flexural modulus, flexural yield strength and compressive yield strength from 5 test parts built in the SLS machine (five tensile, five flexural and five compression).

4.2.1 Tensile properties

Figure 4 shows the ultimate tensile strength (UTS) and results obtained in relation to various energy densities and proportions of filler. From Figure 4a, it is clear that UTS increases rapidly with an increase in ED, except at the highest ED level when the tensile strength decreased steadily. Judging from the results obtained, the ultimate tensile strength was directly influenced by the part-density, which is in turn affected by ED. Density and tensile strength are in direct proportion to each other. Therefore, as the part-density increased, so did the tensile strength, resulting in enhanced fusion of polyamide particles and a decrease in porosity to produce a more compact structure and consequently greater tensile strength. With degradation of the polyamide particles due to excessively high energy density, the tensile strength declined directly.

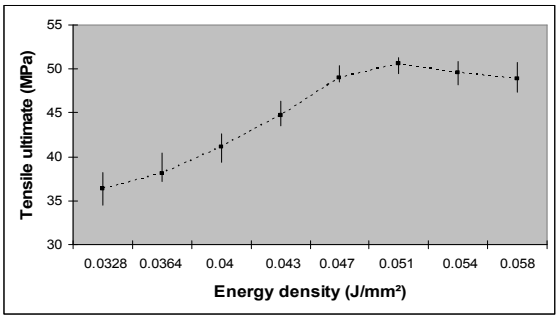

(a)

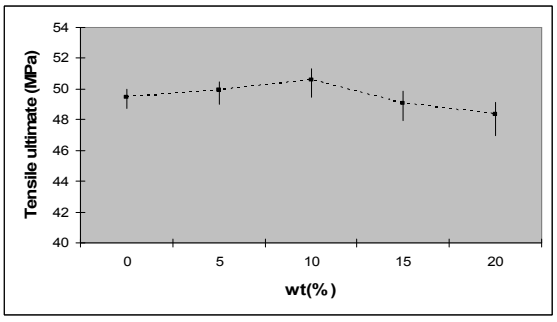

(b)

Figure 4 Variation of tensile ultimate with (a) energy density and (b) cement content

Figure 4b illustrates the dependence of the UTS in the samples on the weight fraction (wt%) of the cement. When wt% is < 10%, the UTS of the composite increases steadily with the addition of wt%, and then decreases gradually with increasing wt%. This suggests that the cement particles can enhance the ultimate tensile strength to some extent and continue to do so as the filler is increased. This is explained by He and Jaing who have presented the percolation theory, which states that a matrix zone around each particle of filler is affected by stress concentration. Consequently, if the particles are fine, well distributed and the distance between them is small enough, it leads to the merging of zones, which increases strength (Mareri, 1998; Unal, 2004). When the filler increases by more than 10%, the gap between the polyamide particles increases, and so the adhesion between the particles will decrease, leading to a reduction in UTS.

4.2.2 Flexural properties

Graphs of the flexural modulus and flexural yield strength values in relation to various energy densities and proportions of filler are shown in Figure 5. The flexural modulus and flexural yield strength values are effectively dependent on the energy density so Figure 5 demonstrates flexural strength which has increased rapidly, as ED has increased to some extent and then decreased as the ED increased. Therefore, it is clear from an examination of the data presented that the ED level used to produce the parts has had a physically powerful influence on the resultant flexural strength value, which can be related back to their density. As the density of the part increases, the flexural properties increase and if the density of the part decreases, the flexural properties also decrease in direct proportion. . As a matter of fact, there is a substantial similarity between the figures of the flexural and the density curves shown in Figure 3d. From the results obtained, it would appear that both the flexural modulus and flexural yield strength were influenced directly by the part-density, which is itself affected by ED. As ED increases, therefore, there is greater fusion of the polyamide particles causing higher density and enabling a more compact structure and consequently more flexural strength. When the ED is increased beyond the optimum level as a consequence of binder degradation, this, however, leads to a decline in strength.

Figure 6 displays the relationship between the flexural strength and weight fraction (wt%) of the cement. It can be seen that the flexural strength increases speedily with the increase of wt% when wt% is < 15%, and then rises gradually. From the

results obtained, this suggests that the cement particles can enhance the flexural strength. Addition of rigid particles like cement to polyamide can increase the stiffness (Gill and Hon, 2004). This means that the flexural strength not only depends on the adhesion of particles to each other, but also on the strength of the particles. Flexural strength, therefore would seem to increase with a rise in the proportion of cement (wt%).

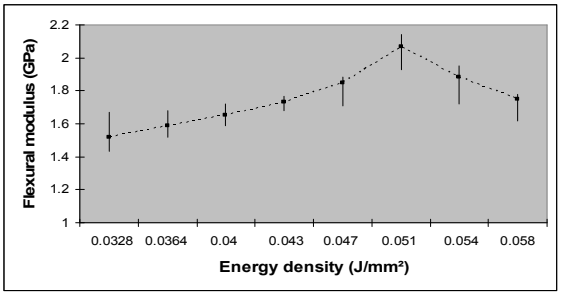

(a)

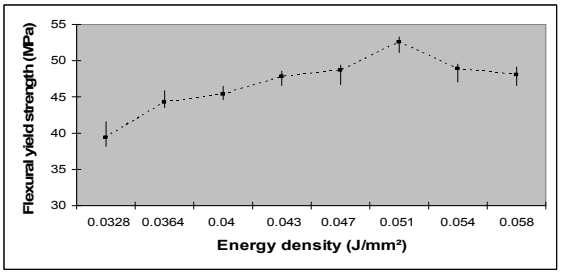

(b)

Figure 5 Variation of energy density with (a) flexural modulus and (b) flexural yield strength

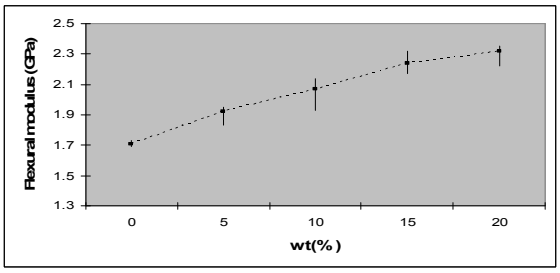

(a)

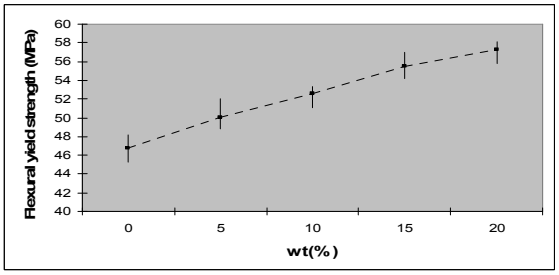

(b)

Figure 6 Variation of cement content with (a) flexural modulus and (b) flexural yield strength

4.2.3 Compression properties

The compression test results are presented in Figure 7. Figure 7a is a chart of compressive yield strength values obtained against various energy densities, where ED is shown to have an effect on the compressive yield strength. It can be seen that the compressive strength quickly increases with an increase in ED when ED is < 0.051, and then decreases slowly. This demonstrates the strength of the relationship between compressive yield strength and density. As the density of the part increases, so does the compressive yield strength caused by more binder particles melting due to a certain degree of increase in ED. The compressive yield strength then starts to decrease as ED is increased as a result of the degradation of binder.

In Figure 7b, the compressive yield strength curve shows considerable influence from various weight fractions (wt%) of the cement. The compressive strength initially increases rapidly with an increase in wt% of up to 5% and then continues more gradually than before. This result confirms that the addition of rigid particles to polyamide enhances rigidity as stated earlier. Consequently, as the (wt%) of the cement increases, so does the compressive yield strength.

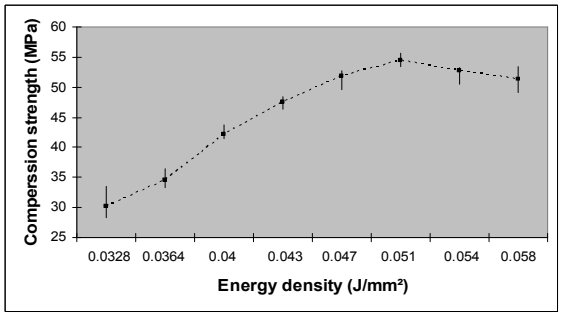

(a)

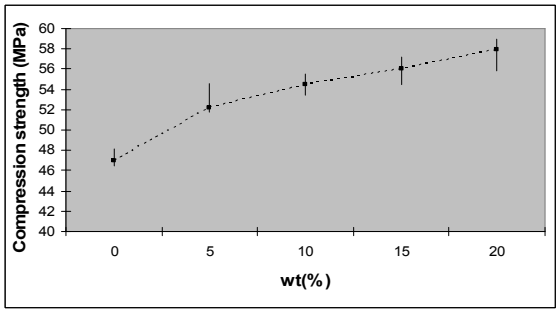

(b)

Figure 7 Variation of compression strength with (a) energy density and (b) cement content

4.3 Morphology and microstructure

In order to carry out this investigation, the material morphology of parts produced from a composite of polyamide and cement SLS has been explored using different energy densities. The research explains the effects of various energy densities on composite material properties by examining the physical construction of the specimens.

Fracture surface images are presented in Figure 8. These fracture surface images of the parts reveal how ED affects the material morphology. From Figure 8a it can be observed that at lower energy densities, there is partially melted polyamide but the majority of particles can be recognized individually because they have maintained their original shape rather than melting. This confirms the findings with respect to the surface image at low ED, which has resulted in the production of a composite part with defects and porosities and so would influence a preference for the stronger specimens. When ED increases beyond 0.047 J/mm², the fusion of particles seems to be homogeneous and particles cannot be seen independently (see Figure 8 b and c). Due to excessive exposure of the energy density to the powder at a level above 0.054 J/mm², Figure 8 d shows degradation of the powder and when the images are enlarged x200, it is also clear that the fracture surfaces are rough. This therefore confirms that findings which relate to surface images where energy density is excessively high, display degradation of the polyamide and a dark colour on the surface of the part due to overheating caused by energy density.

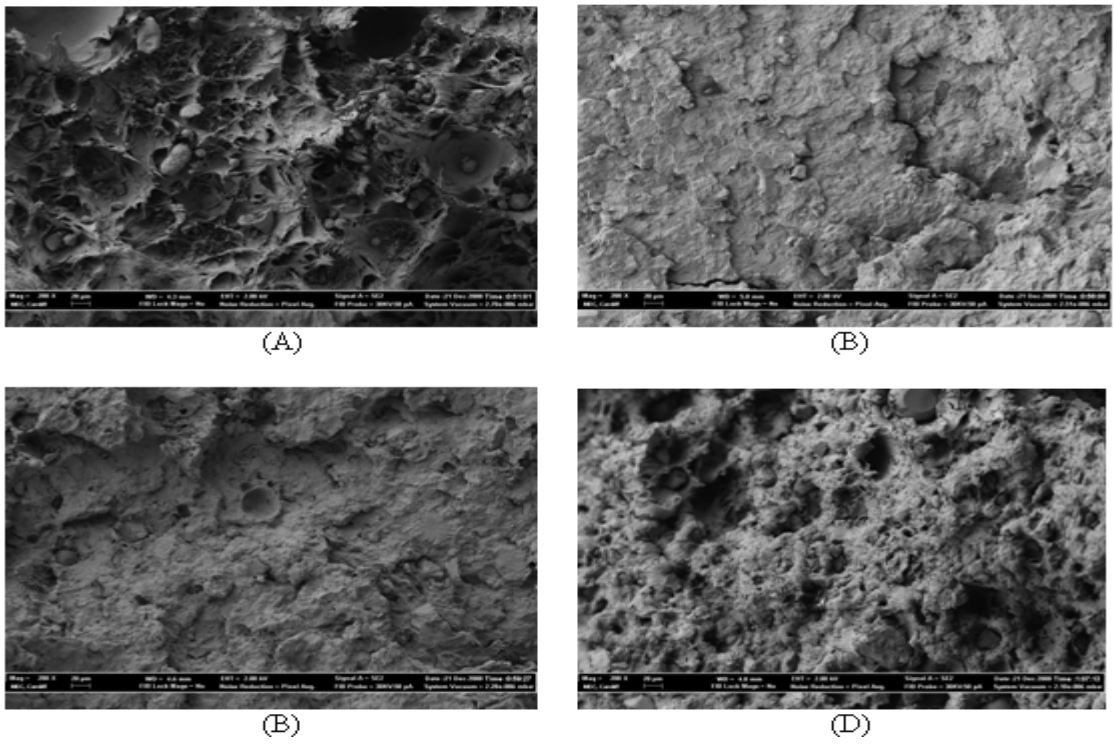

Figure 8 Fracture surface image sintered specimens built at energy density of (a) 0.043, (b) 0.047, (c) 0.051 and (d) 0.054 J/mm²

5 Conclusion

Results from these experiments reveal that the composite material from cement additive and polyamide 12 has a significant effect on the mechanical properties of sintered specimens. Additionally, the ED has a major effect on the dimensions, density and mechanical properties of sintered parts. Compared with pure polyamide 12 powder, the blended powder of polyamide 12 and cement displays improved tensile strength, flexural strength and compression strength of the sintered specimens. The density and mechanical properties are observed to increase as energy density is increased. They peak and then decrease as energy density is increased even further. Sintered parts are porous and weak if the energy density is inferior, but become denser and stronger as energy density increases to a certain degree and then are weakened through degradation of the binder at higher temperatures. This study is considered to have provided new SLS material for the fabrication of functional specimens.

References

Ajoku, U. Saleh, N. Hopkinson, N. Hague, R. and Erasenthiran, P. 2006. Investigating mechanical anisotropy and end-of-vector effect in laser-sintered nylon parts. *I Mech E Proceedings Part B: Journal of Engineering Manufacture.* 220(7) pp 1077-1086.

Beamam, J.B. Barlow, J.W. Bourell, D.L. Crawford, R.H. and Marcus, H.L. 1997. *Solid Freeform Fabrication: A New Direction in Manufacturing.* Dordrecht: Kluwer Academic Publishers.

Caulfield, B. McHugh, P.E. and Lohfeld, S. 2007. Dependence of mechanical properties of polyamide components on build parameters in the SLS process. *Journal of Materials Processing Technology.* 182(1-3) pp 477-488.

Gill, T.J. and Hon, K.K.B. 2004. Experimental investigation into the selective laser sintering of silicon carbide polyamide composites. *I Mech E Proceedings Part B: Journal of Engineering Manufacture.* 218(10) pp 1249-1256.

Hon, K.K.B. and Gill, T.J. 2003. Selective Laser Sintering of SiC/Polyamide Composites. *Journal of CIRP Annals Manufacturing Technology.* 52(1) pp 173-176.

Kai, C.C. and Fai, L.K. 1997. *Rapid Prototyping: Principles & Applications in Manufacturing*. New York: Wiley.

Kumar, V. and Dutta, D. 1997. An assessment of data formats for layer manufacturing. *Journal of Adv. Engng Software* 28(3), pp.151- 164.

Lea, F.M. 1970. *The Chemistry of Cement and Concrete.* 3rd ed. Glasgow: Edward Arnold Ltd.

Maeda, K. and Childs, T.H.C. 2004. Laser sintering (SLS) of hard metal powders for abrasion resistant coatings. *Journal of Materials Processing Technology*. 149(1-3) pp 609–615.

Mareri, P. Bastide, S. Binda, N. and Crespy A 1998. Mechanical Behaviour of Polypropylene Composites Containing Fine Mineral Filler: Effect of Filler Surface Treatment. *Composites Science and Technology.* 58(5) pp 747-752

Neal, P. J. 1994. Rapid Prototyping Using the Selective Laser Sintering Process. *Rapid Prototyping Journal.* 14(2) pp 14-17.

Parnes, P. 1983. *Structure and Performance of Cements*. London: Applied Science.

Pham, D.T. and Dimov, S.S. 2000. *Rapid Manufacturing: The Technologies and Applications of Rapid Prototyping and Rapid Tooling*. London: Springer.

Pham, D. T. and Dimov, S. S. 2003. Rapid Prototyping and Rapid Tooling – the key enablers for rapid manufacturing. *I Mech E Proceedings Part C: Journal of Mechanical Engineering Science* 217(1),pp. 1-23.

Shirley, D.E. 1986. *Introduction to Concrete.* 3rd ed. Slough: Cement and Concrete Association.

Unal, H. 2004. Morphology and mechanical properties of composites based on polyamide 6 and mineral additives. *Materials & Design*. 25(6) pp 483-487.

Vail, N.K. Balasubramanian, B. Barlow, J.W. and Marcus, H.L. 1996. A thermal model of polymer degradation during selective laser sintering of polymer coated ceramic powders. *Rapid Prototyping Journal.* 2(3) pp 24-40.

Yusoff, W.A.Y. 2007. *An investigation of the "Orange Peel" Phenomenon*. PhD Thesis, Cardiff University.